

## Electro, Physical &amp; Theoretical Chemistry

## Supramolecular Self-Assembly of Ionic Discotic Liquid Crystalline Dimer with DNA at Interfaces

Samapika Mallik,<sup>[a]</sup> Alpana Nayak,<sup>\*[a]</sup> Snehasis Daschakraborty,<sup>[b]</sup> Sandeep Kumar,<sup>[c]</sup> and Kattera A. Suresh<sup>[d]</sup>

Nanoarchitectonics through ionic self-assembly at interfaces is an attractive approach to obtain advanced functional materials. Here, a novel discotic dimer-DNA complex hybrid system has been investigated at air-water and air-solid interfaces. The ionic discotic liquid crystalline dimer consisted of two triphenylene cores linked via alkyl spacer with an imidazolium moiety. At air-water interface, the dimer formed a stable monolayer with a reversible collapse. The surface manometry results suggested that the condensed phase of the monolayer consisted of molecules arranged in an edge-on conformation. To understand the folding behavior of the molecules, DFT calculations were

carried out which showed that the quantum chemically optimized folded-form of the molecule was electronically more stable than its unfolded-form. Upon adding DNA to the subphase, a complex monolayer was formed with enhanced stability as was indicated by increased collapse pressure and decreased limiting area. Importantly, this complexation enabled an efficient and stable multilayer formation on silicon substrates with layers as many as 40. Since both DNA and discotic dimer molecules share common properties of one-dimensional charge transport with compatible structures, this complex film could serve as a model system for organic electronics.

## Introduction

Ionic discotic liquid crystals (DLCs) are fundamentally important model systems for studying anisotropic ion-conduction through intriguing supramolecular architectures.<sup>[1,2]</sup> Their long alkyl chains act as an insulating sheet for the ion conduction through well-organized structures such as 1D columnar, 2D smectic or 3D bicontinuous cubic.<sup>[3]</sup> These properties make ionic DLCs suitable for applications in batteries, photovoltaics, electroluminescence and electrochemical devices.<sup>[4]</sup> Being ionic also allow them to self-assemble through electrostatic coupling of structurally different building blocks. One such building block could be a negatively charged naturally occurring polyelectrolyte (i.e., DNA), which can self-assemble with positively charged DLCs and provide a cost-effective approach for large-scale production of supramolecular functional materials.<sup>[5]</sup> The DNA molecule is ubiquitous in nature and has been

an interesting topic of research spanning from biology to technology. Cui et al., about a decade ago, reported the first supramolecular complexation between DNA and asymmetric triphenylene imidazolium salts in the bulk.<sup>[6]</sup> They attributed the well-organized liquid-crystalline phases of DNA-triphenylene complexes to the 1:1 complexation between the phosphate group and the imidazolium salt. They also suggested potential applications of these functional materials in organic microelectronics and gene transfection.<sup>[7]</sup>

The most distinctive feature of DLCs is the  $\pi$ - $\pi$  stacking interaction between the aromatic cores, leading to intriguing supramolecular architectures.<sup>[3]</sup> The more the number of aromatic cores, the stronger will be the stacking interaction. Consequently, DLC dimers that contain two aromatic cores linked via a flexible (or rigid) spacer are expected to demonstrate a higher degree of order compared to their monomeric analogs.<sup>[8]</sup> Further, dimers represent ideal model compounds for polymers and networks.<sup>[9]</sup> Their physical properties are significantly different from the conventional low molar mass DLCs because of restricted molecular motions.<sup>[10]</sup> One of the widely studied systems in this regard is the HBC (hexa-perihexabenzocoronene) derivative.<sup>[11]</sup> While the HBC monomer forms a well-defined columnar mesophase, the HBC dimer fails to do so due to the intermolecular torsion. However, if two HBC units are connected by a sufficiently long and flexible spacer, or if seven HBC units are linked together forming a star-shape, they show interesting hexagonal columnar mesophases.<sup>[12]</sup> There are also other examples of DLC oligomers in literature which form various columnar mesophases and sometimes exhibit very complex phase behavior exclusively due to the  $\pi$ - $\pi$  interaction.<sup>[13]</sup>

So far, most of the studies on DLC oligomers are in the bulk. Studies on the organization of such molecules at the air-

[a] S. Mallik, Dr. A. Nayak  
Department of Physics  
Indian Institute of Technology Patna  
Patna 801103, India  
E-mail: anayak@iitp.ac.in

[b] Dr. S. Daschakraborty  
Department of Chemistry  
Indian Institute of Technology Patna  
Patna 801103, India

[c] Prof. S. Kumar  
Raman Research Institute  
Sadashivanagar, Bengaluru 560 080, India

[d] Prof. K. A. Suresh  
Centre for Nano and Soft Matter Sciences  
Prof. U. R. Rao Road, Jalahalli, Bengaluru 560013, India

Supporting information for this article is available on the WWW under <https://doi.org/10.1002/slct.201800601>

water interface are comparatively rare. Some reports on Langmuir monolayer of a star-shaped DLC oligomer that exhibited a conformation with the peripheral triphenylene subunits sitting perpendicular to, and the central core sitting parallel to the air-water interface, are known.<sup>[14]</sup> A few reports on Langmuir-Blodgett films of DLC dimer, trimer and polymer molecules comprising of chemically connected donor and acceptor subunits are also available.<sup>[15-17]</sup> Particularly, the imidazolium-based DLCs are technologically important because their supramolecular assemblies find applications as heat carriers in solar thermal energy generators and as electrolytes for batteries and capacitors.<sup>[18]</sup> Although some imidazolium-based DLCs are known,<sup>[19]</sup> their dimers and especially, their self-assembly with DNA at interfaces have not yet been studied. Here, first, the supramolecular assembly of an ionic DLC dimer, consisting of two triphenylene cores linked via alkyl spacer with a imidazolium moiety (TplmTp), has been studied at air-water and air-solid interfaces. Next, the ionic self-assembly of TplmTp monolayer and DNA, resulting from non-covalent and electrostatic interactions, have been investigated. For a comparison, the monomer analog of TplmTp has also been investigated. Using DFT calculations, the energetically stable structural conformations of TplmTp dimer have been revealed.

An important aspect of the TplmTp-DNA system is the unique matching in their structures and properties enabling good packing and advanced functions. In the structure of a double-stranded DNA, the distance separating adjacent planes of hydrogen-bonded base pairs is 0.34 nm,<sup>[20]</sup> which is close to the  $\pi$ - $\pi$  stacking distance between two adjacent discotic cores in the columnar mesophase.<sup>[21]</sup> As a consequence, DLCs with interlayer distance of 0.34 nm have been regarded as chemically synthesized version of DNA-mimic.<sup>[22]</sup> On the other hand, DNAs are also known to exhibit liquid crystalline phases.<sup>[23]</sup> Regarding electrical properties, the effective coupling between the  $\pi$ -stack of base pairs is responsible for long-range charge transport in DNA.<sup>[24]</sup> The sugars and phosphates at the periphery of base pairs provide insulation, similar to the long alkyl chains at the periphery of DLCs that provide insulation for one-dimensional charge transport along the column axis. Thus, both DNA and DLCs act as molecular wires. Therefore, complexing DNAs with DLCs through ionic self-assembly at interfaces is a novel approach to develop unique nanoarchitected materials for organic electronics without the need of elaborate covalent chemistry or sophisticated nanotechnology tools.

## Results and Discussion

The material TplmTp in the bulk exhibits the following liquid crystalline phase sequence:<sup>[21]</sup> Solid (S)-columnar phase (Col); 84°C, Col-isotropic (I); 95°C. On cooling, the columnar mesophase appears at 92°C and remains stable down to room temperature. The monomer analog of this material,<sup>[25]</sup> namely, imidazolium tethered with hexaalkoxytriphenylene (ImTp), in the bulk also exhibits similar phase sequence: S-Col; 67°C, Col-I; 101°C. On cooling, the columnar mesophase appears at 98°C with the mesophase solidifying at 38°C.

## Surface manometry

The surface pressure ( $\pi$ ) - area per molecule ( $A_m$ ) isotherms of TplmTp monolayer with ultrapure deionized water subphase and  $10^{-8}$  M concentration of DNA in the subphase are shown in Figure 1A. On pure water, the TplmTp monolayer shows single phase with a limiting area ( $A_0$ ) value of 1.97 nm<sup>2</sup>/molecule. The monolayer collapses at an  $A_m$  of 1.5 nm<sup>2</sup>/molecule with a collapse pressure of about 39 mN/m. The isotherm cycles performed by expanding and compressing the monolayer film at the air-water interface shows reversibility from the collapsed state to the monolayer state with negligible hysteresis (see Supporting Information, Figure S1). For ionic self-assembly with DNA, TplmTp monolayer was formed on water containing DNA at different concentrations. It was observed that, with the increase in concentration of DNA in the subphase, the  $A_0$  value of the isotherm decreases and the collapse pressure increases. Beyond  $10^{-8}$  M concentration of DNA, there was no further change in the isotherm. The  $\pi$  -  $A_m$  isotherm of TplmTp-DNA complex monolayer with  $10^{-8}$  M concentration of DNA in the subphase exhibited a slope change around 1.6 nm<sup>2</sup>/molecule indicating a phase transformation. The  $A_0$  value corresponding to the gradual rise region was 2.3 nm<sup>2</sup>/molecule and steep rise region was 1.56 nm<sup>2</sup>/molecule. The complex monolayer collapsed at an  $A_m$  of 1.2 nm<sup>2</sup>/molecule with a collapse pressure of 47 mN/m. The increased collapse pressure and decreased  $A_0$  value indicates that the presence of DNA in the subphase condenses the TplmTp monolayer film. Unlike pure film, the isotherm cycles performed on the complex film showed irreversible collapse with large hysteresis.

Moreover, the compressional elastic modulus  $|E|$  was calculated<sup>[17]</sup> from the isotherms of both the pure TplmTp monolayer and the TplmTp-DNA complex monolayer using Equation 1.

$$|E| = A_m \left( \frac{d\pi}{dA_m} \right) \quad (1)$$

The  $|E|$  values are particularly useful in understanding the packing of molecules in different phases of a monolayer film. As shown in Figure 1C, the  $|E|$  value showed a maximum of 132.3 mN/m at  $A_m$  of 1.56 nm<sup>2</sup>/molecule for the pure TplmTp monolayer, whereas a maximum value of 163 mN/m at  $A_m$  of 1.26 nm<sup>2</sup>/molecule for the TplmTp-DNA complex monolayer with  $10^{-8}$  M concentration of DNA in the subphase. In addition, the curve showed a hump at 1.94 nm<sup>2</sup>/molecule with a value of 24 mN/m for the complex monolayer. On the basis of these  $|E|$  values, it is inferred that the pure TplmTp monolayer exhibits a condensed phase, whereas, the TplmTp-DNA complex monolayer undergoes a transformation from an expanded phase to a condensed phase.

Because the property of a dimer molecule could be significantly different from that of its monomer analog, similar surface manometry studies were carried out with the monomer ImTp molecule for a comparison. Figure 1B presents the  $\pi$  -  $A_m$  isotherms of the pure monomer ImTp molecule and ImTp-DNA complex monolayer with  $10^{-8}$  M concentration of DNA in the

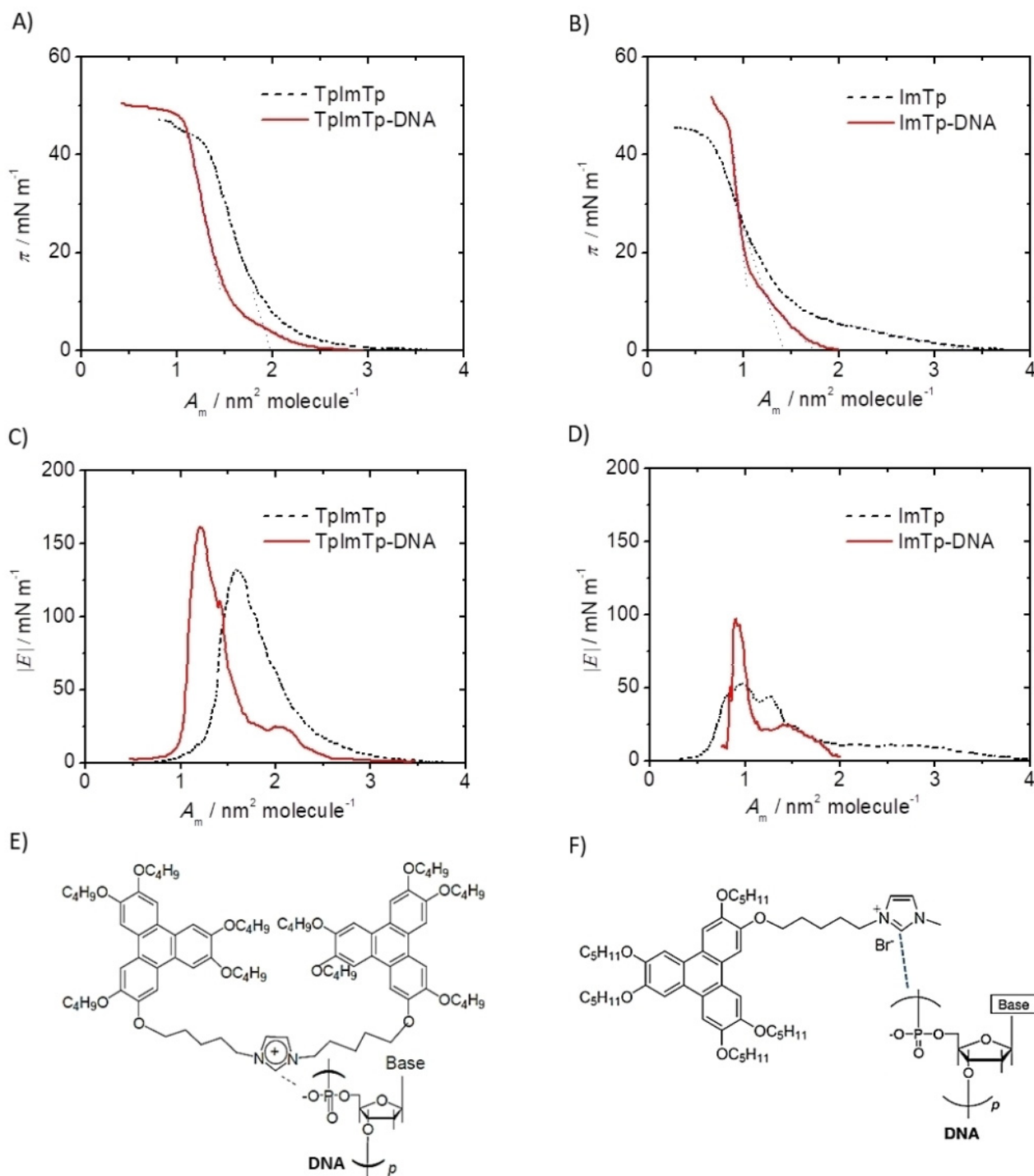


**Figure 1.** (A, B) Surface pressure ( $\pi$ ) - area per molecule ( $A_m$ ) isotherms of dimer TplmTp and monomer ImTp molecules with pure water subphase (dotted line) and  $10^{-8}$  M concentration of DNA in the subphase (solid line). (C, D) Variation of compressional elastic modulus ( $|E|$ ) with  $A_m$  for the isotherms of dimer TplmTp and monomer ImTp with and without DNA in the subphase. (E, F) Chemical structures of TplmTp and ImTp molecules and their interaction with DNA.

subphase. (Notably, the  $10^{-8}$  M concentration of DNA in the subphase was the optimum condition for the formation of a stable complex monolayer. Any further addition of DNA in the subphase did not alter the monolayer properties at the air-

water interface. This was true for both the TplmTp and ImTp molecules.) The  $A_0$  values were 1.40 and 1.11 nm<sup>2</sup>/molecule at the steep-rise region and 3.4 and 1.73 nm<sup>2</sup>/molecule at the gradual-rise region for the pure and the complex monolayers,

respectively. The isotherm cycles showed reversible collapse for the pure monolayer but irreversible collapse for the complex monolayer, similar to that of the dimer system (see Supporting Information, Figure S1). The variation in  $|E|$  values with  $A_m$  (Figure 1D) showed a maximum of 98 mN/m at 0.85 nm<sup>2</sup>/molecule for the complex monolayer and 53.9 mN/m at 0.977 nm<sup>2</sup>/molecule for the pure monolayer. Additionally, the  $|E|$  curves show humps with values of 24.3 mN/m at 1.4 nm<sup>2</sup>/molecule and 12 mN/m at 2.7 nm<sup>2</sup>/molecule corresponding to the gradual rise region of the isotherms of complex and pure monolayers, respectively. Therefore, unlike the dimer TplmTp system, these  $|E|$  values indicate that both ImTp and ImTp-DNA complex monolayers undergo a transformation from an expanded phase to a condensed phase.

### Brewster angle microscopy (BAM)

The TplmTp and the TplmTp-DNA complex monolayer films were observed under BAM while isothermal compression. Figure 2 shows the BAM images for the pure TplmTp mono-

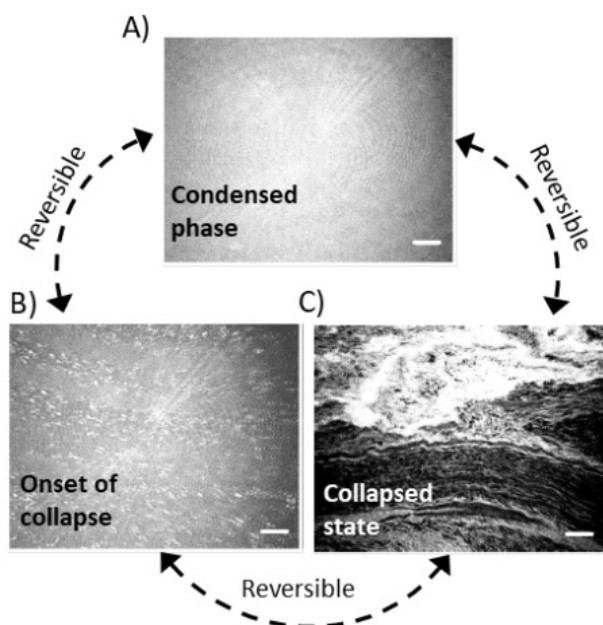


**Figure 2.** Brewster angle microscope images of the TplmTp monolayer at air-water interface with deionized water subphase. (A) Uniform bright intensity indicating a condensed phase at  $A_m = 1.50$  nm<sup>2</sup>/molecule, (B) 3D domains developing over condensed phase indicating the onset of collapse state at  $A_m = 1.20$  nm<sup>2</sup>/molecule, and (C) collapsed state at  $A_m = 0.70$  nm<sup>2</sup>/molecule. The scale bar in each image represents 500  $\mu$ m.

layer. The film exhibited a uniform phase from nearly zero surface pressure. The brightness gradually increased upon compressing the uniform condensed phase (Figure 2A) which transformed to 3D crystals at the collapse state (Figure 2B and 2C). On expansion, these crystalline domains disappeared and the system reverted back to the uniform intensity region indicating a completely reversible monolayer state. Figure 3

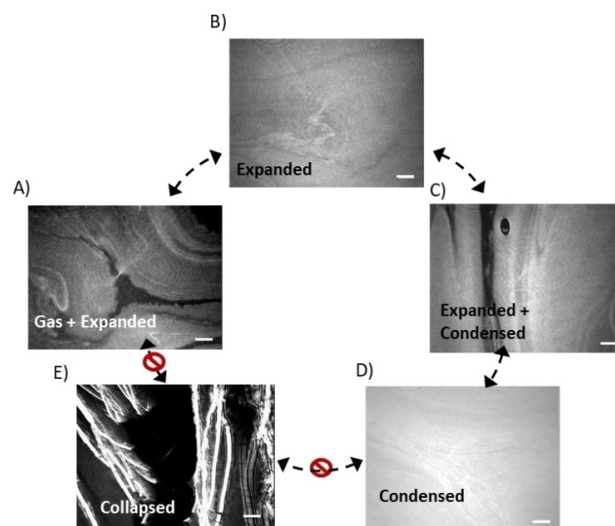


**Figure 3.** Brewster angle microscope images of the TplmTp-DNA complex monolayer at air-water interface with 10<sup>-8</sup> M concentration of DNA in the subphase. (A) Coexistence of gas phase and expanded phase at  $A_m = 2.4$  nm<sup>2</sup>/molecule, (B) expanded phase at  $A_m = 1.75$  nm<sup>2</sup>/molecule, (C) coexistence of expanded and condensed phase at  $A_m = 1.4$  nm<sup>2</sup>/molecule, (D) condensed phase at  $A_m = 1.1$  nm<sup>2</sup>/molecule, and (E) fully collapsed state at  $A_m = 0.7$  nm<sup>2</sup>/molecule. The scale bar in each image represents 500  $\mu$ m.

shows the BAM images for the TplmTp-DNA complex monolayer. At large  $A_m$ , the complex film exhibited a coexistence of gas and expanded phase (Figure 3A). This transformed to a uniform expanded phase upon compression (Figure 3B). At an  $A_m$  of about 1.4 nm<sup>2</sup>/molecule, a condensed phase developed over the expanded phase (Figure 3C and 3D). Further compression led to thread-like 3D domains which appeared at the collapsed state (Figure 3E). On expanding the film, these thread-like domains remained without change and the film did not revert back to the monolayer state indicating irreversibility.

For a comparison, the monomer ImTp and ImTp-DNA complex monolayer films were observed under BAM during compression. Unlike dimer TplmTp system, the monomer ImTp showed a coexistence of expanded phase and condensed phase at large  $A_m$ . Upon compression, this transformed to a uniform condensed phase and then to collapsed state showing 3D domains (see Supporting Information, Figure S2). Upon expansion, these 3D domains reverted back to the uniform monolayer state indicating reversible collapse similar to that of the dimer TplmTp system. However, the ImTp-DNA complex monolayer showed irreversibility similar to the dimer TplmTp-DNA complex system. Thus, the BAM observations support the surface manometry results and confirm the existence of distinct monolayer phases of the monomer and dimer systems.

### Langmuir-Blodgett (LB) film deposition

Several layers of both the dimer TplmTp and the monomer ImTp films were transferred onto silicon substrates by Langmuir-Blodgett (LB) technique at a target surface pressure ( $\pi_t$ ) of 35 mN/m (condensed phase). The efficiency of film deposition

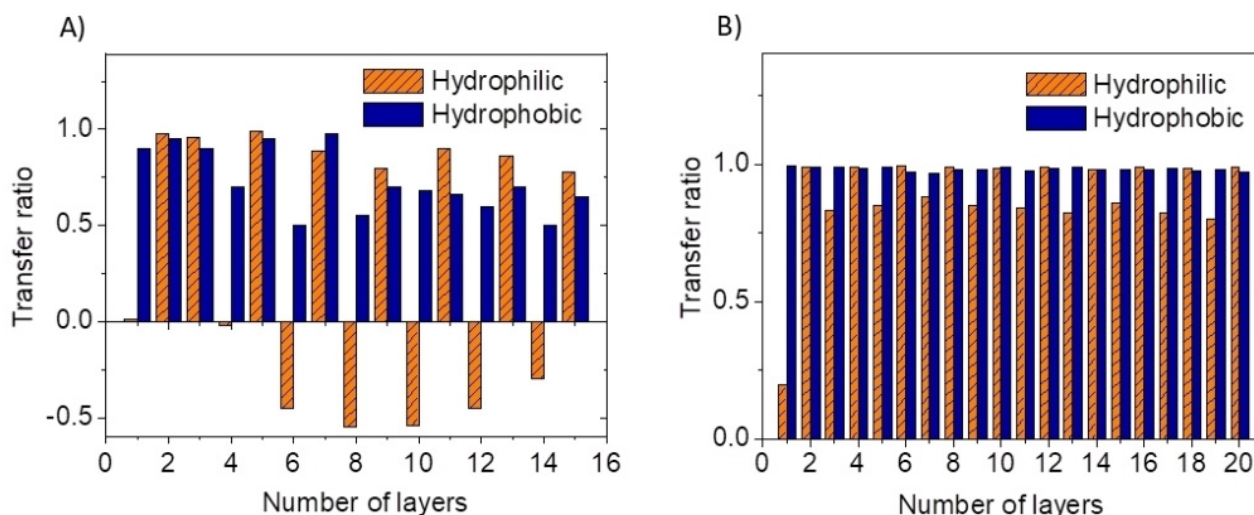


**Figure 4.** Transfer ratio as a function of number of layers of LB film deposition for (A) pure TplmTp monolayer and (B) TplmTp-DNA complex monolayer on hydrophilic and hydrophobic silicon substrates, respectively. The films were transferred at a target surface pressure of 35 mN/m and a dipping speed of 2 mm/min. It can be clearly seen that the transfer ratio is close to 1 indicative of almost perfect deposition for the complex system, whereas the pure system suffers from alternate adsorption and desorption over successive layers of deposition.

was estimated from the transfer ratio ( $\tau$ ) which was calculated by the ratio of the area of the monolayer removed to the area of the substrate coated. A  $\tau$  of unity is indicative of good deposition. The  $\tau$  data of the LB films of the pure TplmTp with 15 layers on hydrophilic and hydrophobic silicon substrates are shown in Figure 4A. For the hydrophilic substrate, an alternate desorption and adsorption after the first two layers of deposition was observed. For hydrophobic substrate, the transfer was efficient only for the first few layers. Thus, for the pure TplmTp dimer film, multilayer formation was not very efficient. However, when the TplmTp film was complexed with DNA ( $10^{-8}$  M concentration in the subphase), the transfer efficiency increased remarkably as shown in Figure 4B. On hydrophilic substrate, the  $\tau$  value was close to 1 for every upstroke and was slightly less (ranging between 0.9 to 0.7) for every downstroke of film deposition. Interestingly, on hydrophobic substrate, the  $\tau$  value was close to 1 for both the up and down strokes and continued with the same efficiency for several tens of layers. Furthermore, the  $\tau$  data collected for the monomer ImTp system also showed deposition only for the first few layers and multilayers could not be formed. Although the ImTp-DNA complex film formed multilayers, they were not as efficient as that of the dimer TplmTp-DNA complex film.

The observed differences in deposition may be attributed to the molecule-molecule and the molecule-substrate interactions together with the effect of flow patterns of the subphase near the meniscus region during the up and down strokes.<sup>[26]</sup> The deposition of charged monolayer involves complicated physical and chemical processes controlling the efficiency of film deposition. Both the dimer TplmTp and the monomer ImTp have cationic imidazolium polar head group with  $\text{Br}^-$  as counterion. When these molecules form monolayer at the air-water interface, the small  $\text{Br}^-$  counterions dissolve into the subphase due to the dissociation of the ionic groups.

The presence of these  $\text{Br}^-$  counterions in the subphase and the positively charged monolayer at the surface form an electric double layer at the air-water interface. These  $\text{Br}^-$  counterions might not be sufficient enough to compensate the charge of the monolayer during deposition. It is quite possible that concentration polarization would have developed leading to meniscus instability, thereby disrupting the multilayer formation. On contrary, addition of small amount of DNA ( $\sim 10^{-8}$  M conc.) in the subphase suppresses the concentration polarization effect, thereby facilitating stable multilayer formation. This is evident from the high transfer efficiency ( $\tau \sim 1$ ) observed for the deposition of the complex films. It is worth mentioning that van der Waals forces also play significant role in the adhesion of monolayers, but for the charged monolayer deposition, its contribution is much smaller than the double layer repulsive contribution.<sup>[27]</sup>

#### Atomic force microscopy (AFM)

To understand the organization of molecules at different phases of the isotherm, AFM imaging of monolayer and multilayer films transferred at different  $\pi_t$  were carried out for both the pure and complex films. Topography images of the pure TplmTp LB-film with different layers transferred onto silicon substrates at a  $\pi_t$  of 35 mN/m are shown in Figure 5. The film with single layer on a hydrophilic substrate exhibited a uniform surface and was scratched with AFM tip to reveal the actual thickness of about 2 nm (Figure 5A). The films with 2, 4 and 8 layers on hydrophobic substrates revealed thicknesses of about 4, 8 and 16 nm respectively (Figure 5B, 5C and 5D). The roughness and irregularities in film morphology may be attributed to factors like reorganization of molecules in the film during the transfer process, natural dewetting of the film,

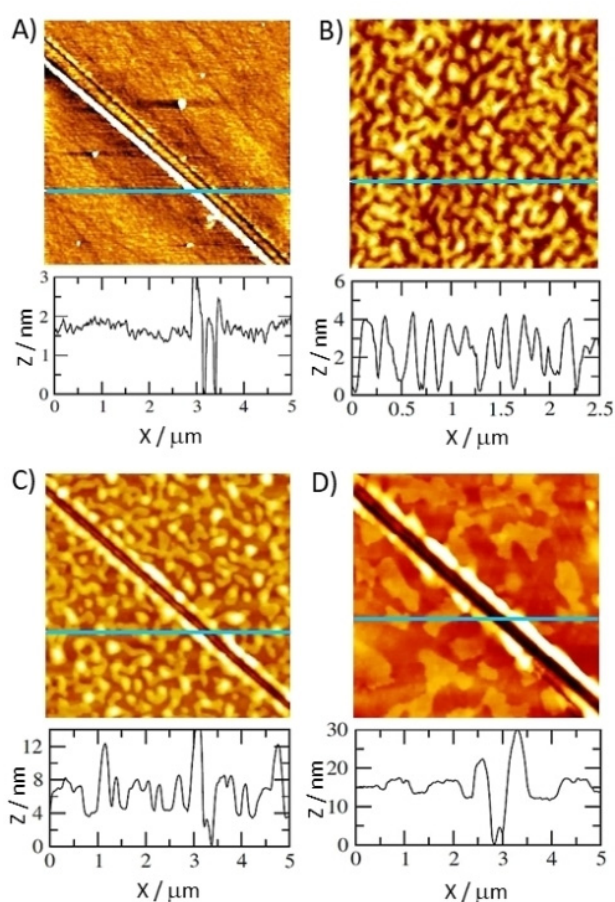


**Figure 5.** AFM topography images of pure TplmTp LB films transferred onto silicon substrates in the condensed phase at a  $\pi_t$  of 35 mN/m with (A) 1 layer, (B) 2 layers, (C) 4 layers, and (D) 8 layers. The films are scratched with the AFM tip to find the actual height. The respective height profiles corresponding to the lines drawn on the images are shown below.

evaporation of entrapped water within the layers and varying transfer efficiency for different layers of deposition.

For the TplmTp-DNA complex film, the images of single layer transferred at  $\pi_t$  values of 10, 35 and 55 mN/m onto hydrophilic silicon substrates are shown in Figure 6A, 6B and 6C respectively. At 10 mN/m, the film was not compact and showed a height of about 0.5 nm corresponding to the expanded phase. At 35 mN/m, the film was compact corresponding to the condensed phase, and was scratched to reveal a thickness of about 2.4 nm. The film transferred at 55 mN/m showed thread-like domains of the collapsed state, similar to those observed in the BAM images. Further, TplmTp-DNA complex film with 2, 4 and 8 layers were transferred onto hydrophobic silicon substrates as shown in Figure 6D, 6E and 6F, respectively. The line profiles drawn on the images give information about the roughness of the film but not the actual film thickness. Since all of these films were compact, they were scratched with AFM tip which revealed the actual thicknesses of slightly greater than 4, 8 and 16 nm, respectively, due to the presence of DNA. Additional images of scratched films are shown in the Supporting Information (Figure S3).

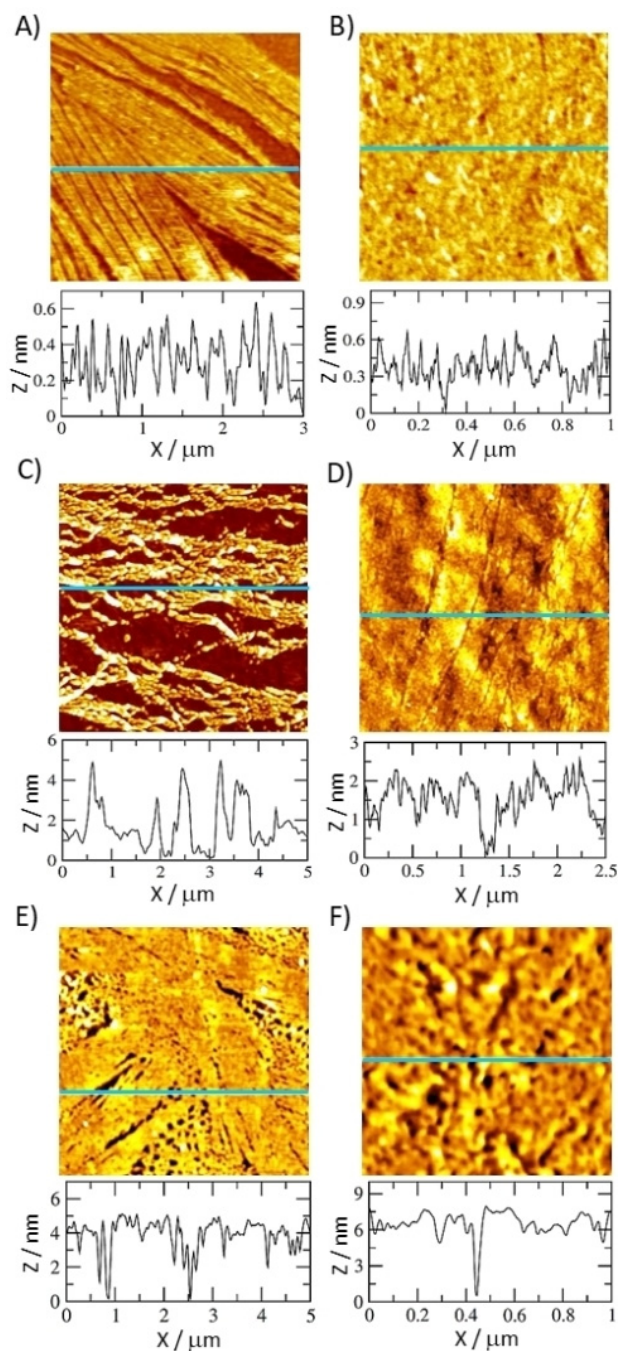


**Figure 6.** AFM topography images of TplmTp-DNA complex LB film with 1 layer in the (A) expanded phase ( $\pi_t = 10$  mN/m), (B) condensed phase ( $\pi_t = 35$  mN/m), and (C) collapsed state ( $\pi_t = 55$  mN/m). Multilayer films transferred in the condensed phase at a  $\pi_t = 35$  mN/m with (D) 2 layers, (E) 4 layers and (F) 8 layers. The respective height profiles of the film surface corresponding to the line drawn are shown below each images.

Interestingly, no thread-like structures were observed in the multilayered films of the TplmTp-DNA complex unlike those observed in a previous study of a discotic PyTp-DNA complex system.<sup>[28]</sup> Even in the case of monomer ImTp-DNA complex film with 20 layers, no such thread-like features were seen. However, the presence of DNA was confirmed by Fourier

transform infrared spectroscopy on these films which showed characteristic absorption bands of DNA molecules. DNA does play an important role to obtain almost perfect transfer ratio for the formation of stable multilayers on a substrate. Apparently, the amount of DNA molecules themselves getting transferred to the substrate depends on the cationic polar head group of the discotic amphiphile. In the previous study of PyTp-DNA system,<sup>[28]</sup> the polar head group was a pyridinium moiety. For a pyridine moiety, the replacement of a CH in the benzene ring by more electronegative nitrogen atom induces a dipole moment of 2.2 D, denoting a shift of electron density from the ring towards the nitrogen atom.<sup>[29]</sup> (Benzene molecule which is symmetrical has zero dipole moment.) For ImTp and TplmTp molecules, the polar head group is a imidazolium moiety. In an imidazole moiety, the replacement of CH by electronegative nitrogen atom at two positions, induces a dipole moment of 3.61 D.<sup>[30]</sup> The valence bond (resonance) description indicates that both the pyridinium ring and the imidazolium ring have delocalized positive charge.<sup>[31]</sup> Although DNA complexation is primarily electrostatic in nature, experimental observation indicates that the pyridinium polar head group is more effective in transferring DNA than the imidazolium group. Understanding the reason behind this is open for future investigations.

On the basis of surface manometry results and AFM images, the conformation of the TplmTp dimer molecule in the monolayer film can be suggested. From molecular dimensions, the TplmTp dimer molecule on a surface has  $A_o$  values of 8.6 nm<sup>2</sup>/molecule and 1.46 nm<sup>2</sup>/molecule for the face-on and edge-on conformations, respectively (Figure 7A and 7B). Experimentally, both BAM and isotherm showed a single condensed phase for the TplmTp monolayer with a corresponding  $A_o$  value of 1.97 nm<sup>2</sup>/molecule. The AFM image of TplmTp monolayer film transferred at the condensed phase (35 mN/m) showed a height of 2 nm. Comparing the film height and the  $A_o$  value with the molecular dimensions, this condensed phase appears to be composed of molecules arranged in an edge-on conformation. Due to the electrostatic repulsion between the molecules, the  $A_o$  value obtained from the surface manometry measurements was larger than the theoretically estimated value.

Since the physical properties of discotics that are essential for device applications can be tailored, the alignment of molecules in thin films has been an important topic of research over the past several decades.<sup>[32–34]</sup> Depending upon the molecule-molecule and molecule-substrate interactions, discotics are known to exhibit interesting molecular conformations on a substrate. Perova *et al.* observed the anchoring transition (similar to the local Fredericks transition) in discotic liquid crystals from the edge-on to the face-on (side-on) alignment for a number of substrates both untreated and coated with polymer.<sup>[34]</sup> Using infrared dichroic ratio, they also showed explicitly that the cores of triphenylene align face-on (i.e., side-on) to the Si-substrates.<sup>[32]</sup> They inferred from these observations that the condition of the minimum surface energy is fulfilled if the director (axis of the column) has a planar orientation (i.e. edge-on alignment) and this type of alignment

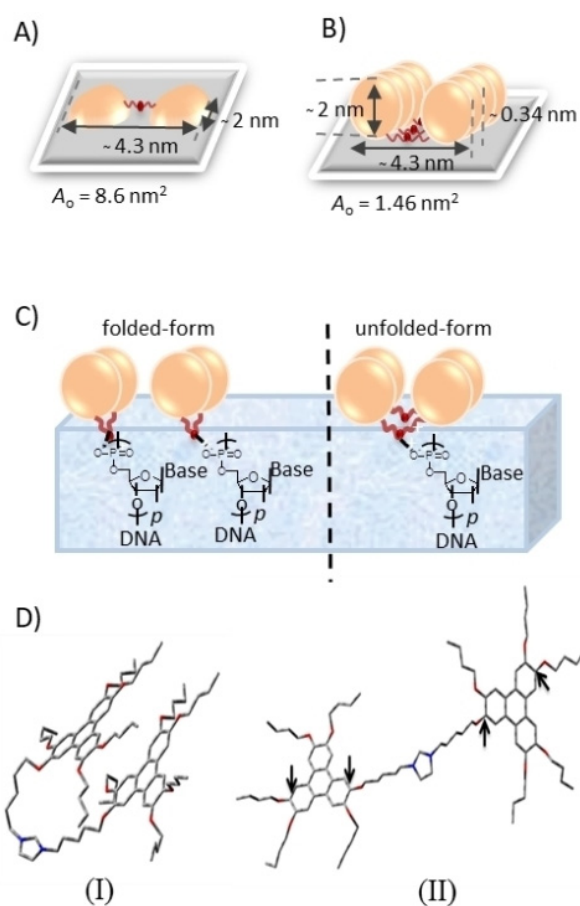


**Figure 7.** Schematic diagram of the possible conformations of TplmTp molecules on a surface. (A) Face-on. (B) Edge-on. (C) Folded- and unfolded-forms of edge-on conformation. The  $A_o$  values are estimated based on the molecular dimensions and configurations. (D) Two quantum chemically optimized conformers of the molecule: (I) the folded-form and (II) the unfolded-form. The H atoms are not shown for clarity.

for the discotic LC is normally preferred. Moreover, whether this alignment has a homogeneous or heterogeneous character depends on whether or not a substrate has one or more than one easy direction of orientations. Microscopically, the contributions to the anchoring energy were attributed to the topology, steric, polar and dispersive (caused by van der Waals) interactions.

In the present work, the film is formed on the surface of water. In general, the anchoring of discotic molecules on water surface could be face-on or edge-on depending on the availability of surface area and anchoring sites (polar groups) per molecule (Figures 7A and 7B). At larger surface area per molecule, they tend to align in a face-on conformation, whereas at smaller surface area per molecule, they align in an edge-on conformation. The transition between these two conformations occur reversibly during symmetric compression and expansion of the monolayer as shown in the isotherm cycle for the monomer molecule (Figure S1). However, the dimer molecules exhibit only edge-on conformation due to the strong pi-pi interaction between their cores. Interestingly, these

conformations were preserved when monolayer films were transferred from water surface to solid substrate indicating high stability. This was confirmed by the height information extracted from the AFM topography images of the films transferred on solid substrate. Similar observations were also reported in our previous work.<sup>[35]</sup>

### DFT calculations

Further insight into the molecular conformation was sought through DFT calculations. For discotic dimers, the edge-on conformation could be of two types, namely, folded- and unfolded-form as shown in Figure 7C. Particularly, if the two discotic cores of the dimer are connected by flexible spacer, they tend to fold due to the strong  $\pi$ - $\pi$  interactions.<sup>[36–38]</sup> In the present work, the TplmTp dimer molecule is symmetric and the experimentally observed  $A_0$  values only indicate an edge-on conformation without clarifying whether or not it is folded. In order to study the folding behavior of the molecule, first-principles calculations were carried out based on density-functional theory (DFT) at B3LYP/6-311G\*\* level and basis set. It is known that DFT does not handle the dispersion interaction accurately.<sup>[39,40]</sup> The  $\pi$ -stacking interaction energy is generally underestimated. Therefore, the structures resulted from the above DFT calculation were re-optimized using a new functional B97-D developed by Grimme with D95(d,p) basis set. Despite the fact that the above combination is less computationally expensive, it provides good optimized geometry with more accurate dispersion interaction. This calculation scheme has been called as DFT–D hereafter. Figure 7D shows the optimized structures of the folded (I) and the unfolded (II) forms of the molecule. These structures were obtained by unconstrained geometry optimizations starting from a variety of extended and folded conformations. The coordinates of the atoms for the two forms are given in Table S1 and S2 of the Supporting Information. Table 1 presents energy values and the

electronically stable by  $\sim 12.62$  kcal/mol over its unfolded form, the DFT–D calculation predicts much stronger folding interaction energy of  $\sim 40$  kcal/mol. Also, the DFT calculation predicts folded form (I) as a parallel-displaced conformer, having  $\pi$ - $\pi$  stacking interaction with certain inter-disk separation. The distance between the two center of mass of the aromatic segments were estimated to be 5.4 Å and 23.6 Å, and the perpendicular distance between the two aromatic planes were estimated to be 4.2 Å and 1.2 Å for the folded- and the unfolded-forms, respectively, from DFT calculations. However, the DFT–D calculation predicts a smaller inter-disk separation of  $\sim 3.0$  Å for the folded-form and 0.6 Å for the unfolded-form. This large difference between the results obtained from the DFT–D and the DFT calculations is consistent with earlier studies.<sup>[41,42]</sup> However, this difference may change slightly upon considering bigger basis set, which is pretty difficult for the current system.

This model is in good qualitative agreement with the experimental results of film heights from AFM imaging and limiting area from surface manometry corresponding to the edge-on configuration. Moreover, the fact that the folded form is energetically more stable than the unfolded form is in line with the previous reports in literature on similar systems. For instance, modelling done by Boden *et al.* suggested that the steric crowding in dimers makes conformations in which both discotic cores are coplanar unlikely.<sup>[36]</sup> In another study, Bozek *et al.* reported that folding allowed the dimers to assemble into a columnar liquid crystal phase, despite their short linking group.<sup>[37]</sup> Recently, it has also been shown for discotic dyads that the folded-form is significantly more stable than the unfolded-form.<sup>[38]</sup>

Thus, this study deals with the interfacial nanoarchitecture of a novel discotic dimer and its complexation with DNA. This approach is suitable for a cost-effective and large-scale production of technologically important supramolecular hybrid films without the need of elaborate covalent chemistry or complicated nanotechnology tools. In literature, DNA-cationic surfactant complexes are known as advanced materials with unique mechanical, electrical, optical, and biological properties for specific applications.<sup>[43]</sup> In the present study, the compelling rationale for the building blocks being examined, viz., DNA and discotic, is twofold: Firstly, both exhibit one-dimensional charge transport. Secondly, they have compatible structures. Moreover, DNA being polyelectrolyte provides additional benefit of improved deposition through LB technique. Such hybrid films could be model system for organic electronics. Charge transport measurements, i.e., current as a function of applied field, have already been carried out in a previous report on similar system.<sup>[44]</sup> Future research endeavour, using the present system, is to explore organic atomic-switch based neuromorphic device applications.<sup>[45,46]</sup> The discotic-DNA complex film, when sandwiched between an electrochemically active metal (Ag) and an inert metal (Pt), is expected to show resistance switching due to electrochemical metallization. One of the preliminary results of current-voltage (I–V) switching measurements using conducting AFM is presented in the Supporting Information (Figure S4). A detailed study in this direction is underway.

**Table 1.** Energy values and structural data obtained from first-principles calculations for comparison between the folded and unfolded forms of the TplmTp molecule.

Parameters	Method	Folded Form (I)	Unfolded Form (II)
Relative Energies (setting the energy of form II is zero)	DFT	12.6 kcal/mol	0.0000
	DFT-D	40.0 kcal/mol	0.0000
Distance between the two center of mass of the aromatic segments	DFT	5.4 Å	23.6 Å
	DFT-D	5.0 Å	23.5 Å
Perpendicular Distance between the two aromatic planes	DFT	4.2 Å	1.2 Å
	DFT-D	3.0 Å	0.6 Å
Dihedral angle between the high-lighted atoms (See Figure 7)	DFT	4.24°	124°
	DFT-D	-5.07°	14°

structural data for comparison between these two optimized structures. It is evident from Table 1 that while the DFT calculation predicated the folded form of the molecule is

## Conclusions

The ionic discotic liquid crystalline dimer (TpmTp) forms stable Langmuir monolayer with reversible collapse. As compared to its monomer ImTp analog, the dimer TpmTp monolayer exhibits much higher compressional elastic modulus, indicating a better packing of molecules due to two aromatic cores. DFT-D calculations show that the quantum chemically optimized conformation with the folded-form of the dimer molecule is electronically stable by 40 kcal/mol over its unfolded form, which is consistent with the experimentally obtained limiting area of the TpmTp molecules. Upon adding appropriate amount of DNA in the subphase, the ionic self-assembly of the TpmTp monolayer with DNA results in a decrease in limiting area and an increase in collapse pressure indicating enhanced stability. Interestingly, DNA complexation facilitates an efficient multilayer formation of the TpmTp-DNA system on substrates, indicating the potential for device applications. This work highlights the fact that ionic self-assembly at interfaces is an efficient nanoarchitectonic approach for the designing of advanced functional materials.

## Supporting Information Summary

The supporting information contains detailed experimental section, results of isotherm cycles, additional BAM images, additional AFM images and current - voltage spectroscopy data, and tables of cartesian coordinates of atoms of the optimized structures obtained in quantum chemical modelling.

## Acknowledgment

Authors acknowledge Dr. S. K. Pal at IISER, Mohali, India, for the synthesis of the discotic molecules during his PhD at RRI, Bangalore.

## Conflict of Interest

The authors declare no conflict of interest.

**Keywords:** discotic dimer · discotic-DNA complex · ionic self-assembly · Langmuir-Blodgett films

- [1] K. Goossens, K. Lava, C. W. Bielawski, K. Binnemans, *Chem. Rev.* **2016**, *116*, 4643.
- [2] T. Wöhrle, I. Wurzbach, J. Kirres, A. Kostidou, N. Kapernaum, J. Litterscheidt, J. C. Haenle, P. Staffeld, A. Baro, F. Giesselmann, S. Laschat, *Chem. Rev.* **2016**, *116*, 1139.
- [3] L. A. Haverkate, M. Zbiri, M. R. Johnson, B. Deme, F. M. Mulder, G. J. Kearley, *J. Phys. Chem. B* **2011**, *115*, 13809.
- [4] T. Kato, M. Yoshio, T. Ichikawa, B. Soberats, H. Ohno, M. Funahashi, *Nat. Rev. Mater.* **2017**, *2*, 17001.
- [5] K. Binnemans, *Chem. Rev.* **2005**, *105*, 4148.
- [6] L. Cui, J. Miao, L. Zhu, *Macromolecules* **2006**, *39*, 2536.
- [7] L. Cui, L. Zhu, *Langmuir* **2006**, *22*, 5982.
- [8] a) Y. Wang, C. Zhang, H. Wu, J. Pu, *J. Mater. Chem. C* **2014**, *2*, 1667; b) M. Gupta, S. K. Pal, *Langmuir* **2016**, *32* (4), 1120.
- [9] a) M. Gong, Q. Yu, S. Ma, F. Luo, R. Wang, D. Chen, *Macromolecules* **2017**, *50*, 5556; b) B. Mu, X. Hao, J. Chen, Q. Li, C. Zhang, D. Chen, *Polym. Chem.* **2017**, *8*, 3286.
- [10] C. W. Ong, Y.-Chi Chan, M.-Che Yeh, H.-Ying Lin, H.-Fu Hsu, *RSC Adv.* **2013**, *3*, 8657.
- [11] S. Ito, P. T. Herwig, T. Bohme, J. P. Rabe, W. Rettig, K. Mullen, *J. Am. Chem. Soc.* **2000**, *122*, 7698.
- [12] L. Zhi, J. Wu, K. Mullen, *Org. Lett.* **2005**, *7*, 5761.
- [13] a) M. D. Watson, F. Jackel, N. Severin, J. P. Rabe, K. Mullen, *J. Am. Chem. Soc.* **2004**, *126*, 1402; b) K. Hatsusaka, N. Kimura, K. Ohta, *Bull. Chem. Soc. Jpn.* **2003**, *76*, 781.
- [14] N. C. Maliszewskij, P. A. Heiney, J. Y. Josefovowicz, T. Plesniviy, H. Ringsdorf, P. Schuhmacher, *Langmuir* **1995**, *11*, 1666.
- [15] a) V. V. Tsukruk, H. Bengs, H. Ringsdorf, *Langmuir* **1996**, *12*, 754; b) V. V. Tsukruk, D. Janietz, *Langmuir* **1996**, *12*, 2825.
- [16] B. Kumar, K. A. Suresh, S. K. Gupta, S. Kumar, *J. Chem. Phys.* **2010**, *133*, 044701.
- [17] R. K. Gupta, V. Manjuladevi, C. Karthik, S. Kumar, K. A. Suresh, *Colloids Surf. A: Physicochem. Eng. Aspects* **2012**, *410*, 9.
- [18] S. Sergeev, V. Pisula, Y. H. Geerts, *Chem. Soc. Rev.* **2007**, *36*, 1902.
- [19] a) J. Motoyanagi, T. Fukushima, T. Aida, *Chem. Commun.* **2005**, *1*, 101; b) S. Kumar, S. K. Gupta, *Tetrahedron Lett.* **2010**, *51*, 5459.
- [20] J. C. Genereux, J. K. Barton, *Chem. Rev.* **2010**, *110*, 1642.
- [21] S. K. Pal, S. Kumar, *Tetrahedron Lett.* **2006**, *47*, 8993.
- [22] Jung-Il Jin, J. Grote (Eds.) *Materials Science of DNA*, CRC Press, Taylor & Francis, **2012**.
- [23] a) I. W. Hamley, *Soft Matter* **2010**, *6*, 1863; b) M. Nakata, G. Zanchetta, B. D. Chapman, C. D. Jones, J. O. Cross, R. Pindak, T. Bellini, N. A. Clark, *Science* **2007**, *318*, 1276.
- [24] J. D. Slinker, N. B. Muren, S. E. Renfrew, J. K. Barton, *Nat. Chem.* **2011**, *3*, 228.
- [25] S. Kumar, S. K. Pal, *Tetrahedron Lett.* **2005**, *46*, 2607.
- [26] J. N. Israelachvili, *Intermolecular and Surface Forces*, Academic Press, London, **1992**.
- [27] a) V. I. Kovalchuk, M. P. Bondarenko, E. K. Zholkovskiy, D. Vollhardt, *J. Phys. Chem. B* **2003**, *107*, 3486; b) V. I. Kovalchuk, E. K. Zholkovskiy, N. P. Bondarenko, D. Vollhardt, *J. Phys. Chem. B* **2001**, *105*, 9254.
- [28] A. Nayak, K. A. Suresh, *J. Phys. Chem. B* **2008**, *112*, 2930.
- [29] B. A. Middleton, J. R. Partington, *Nature* **1938**, *141*, 516.
- [30] B. B. DeMore, W. S. Wilcox, J. H. Goldstein, *J. Chem. Phys.* **1954**, *22*, 876.
- [31] M. Sainsbury, *Heterocyclic Chemistry*, Royal Society of Chemistry, Great Britain, **2001**.
- [32] T. S. Perova, J. K. Vij, *Adv. Mater.* **1995**, *7*, 919.
- [33] Z. H. Al-Lawati, R. J. Bushby, S. D. Evans, *J. Phys. Chem. C* **2013**, *117*, 7533.
- [34] T. S. Perova, J. K. Vij, A. Kocot, *Euro Phys. Letts.* **1998**, *44*, 198.
- [35] A. Nayak, K. A. Suresh, S. K. Pal, S. Kumar, *J. Phys. Chem. B* **2007**, *111*, 11157.
- [36] N. Boden, R. J. Bushby, A. N. Cammidge, A. El-Mansoury, P. S. Martina, Z. Lua, *J. Mater. Chem.* **1999**, *9*, 1391.
- [37] K. J. A. Bozek, V. E. Williams, *Soft Matter* **2014**, *10*, 5749.
- [38] M. Gupta, S. P. Gupta, M. V. Rasna, D. Adhikari, S. Dhara, S. K. Pal, *Chem. Commun.* **2017**, *53*, 3014.
- [39] a) S. Grimme, *Angew. Chem. Int. Ed.* **2008**, *47*, 3430; b) S. Grimme, *J. Comput. Chem.* **2006**, *27*, 1787.
- [40] S. Grimme, J. Antony, S. Ehrlich, H. Krieg, *J. Chem. Phys.* **2010**, *132*, 154104.
- [41] D. J. Lacks, R. G. Gordon, *Phys. Rev. A* **1993**, *47*, 4681.
- [42] J. A. Plumley, J. J. Dannenberg, *J. Comput. Chem.* **2011**, *32*, 1519.
- [43] S. Zhou, B. Chu, *Adv. Mater.* **2000**, *12*, 545.
- [44] A. Nayak, K. A. Suresh, *Phys. Rev. E* **2008**, *78*, 021606.
- [45] A. Nayak, T. Ohno, T. Tsuruoka, K. Terabe, T. Hasegawa, J. K. Gimzewski, M. Aono, *Adv. Funct. Mater.* **2012**, *22*, 3606.
- [46] K. Krishnan, M. Muruganathan, T. Tsuruoka, H. Mizuta, M. Aono, *Adv. Funct. Mater.* **2017**, *27*, 1605104.

Submitted: March 1, 2018

Accepted: June 25, 2018